PROPOSAL No. 347

Scientific Spokesman:

James K. Walker
Fermi National Accelerator Lab
P. O. Box 500
Batavia, Illinois 60510

PROPOSAL TO MEASURE THE ELASTIC SCATTERING OF HADRONS AT LARGE MOMENTUM TRANSFER

D. Carey, R. Kammerud, D. Ritchie,
J. Sauer, R. Shafer, D. Theriot, and J. K. Walker
Fermi National Accelerator Laboratory
Batavia, Illinois 60510

and

J. Johnson
Northeastern University
Boston, Massachusetts 02115

and

F. E. Taylor
Northern Illinois University
DeKalb, Illinois 60115

ABSTRACT

We propose measuring cross sections for elastic scattering of $\pi^{\pm}$, $K^{\pm}$, and $\bar{p}$ on protons for values of the four-momentum transfer squared t from -2 to -15 $(GeV/c)^2$ and incident energies of 50, 100, 200, 300 and 400 GeV. Both the forward scattered and recoil particles will be detected in magnetic spectrometers with large acceptance.

TABLE OF CONTENTS

		Page
I.	Introduction	1
II.	Physics Objectives and Justification	2
III.	Experimental Method	6
	A. General	6
	B. Recoil Spectrometer	8
	C. Forward Spectrometer	10
	D. Trigger	12
IV.	Beam Requirements	14
V.	Elastic Rates	15
VI.	Backgrounds	16
	A. Quasi-Elastic N* Production	16
	B. Singles Rates	17
	C. Trigger Rate	19
VII.	Time Request	21
VIII.	Fermilab Request	22
IX.	Proposed Schedule	23
X.	Additional Experimental Possibilities	23
	A. Backward Elastic Scattering	23
	B. Inclusive Reactions	24
APPENDIX I	Magnetic Parameters and Cost Estimate	26
APPENDIX II	Electronic Data Filter and Processor Description	28

I. Introduction

The successful operations of the ISR and the Fermilab Accelerator have allowed the exploration of various hadron reactions at large momentum transfer. The inclusive production of pions has been studied most extensively. The invariant cross sections for these inclusive processes have been found to scale over the entire energy range available at the Fermilab out to several GeV/c transverse momentum.[1] This simple limiting behavior has been observed when the cross section is expressed in terms of the radial variable $x_R = 2E^*/\sqrt{s}$ rather than the Feynman variable $X_{\parallel} = 2P_{\parallel}{}^*/\sqrt{s}$ where $P_{\parallel}{}^*$ and E^* refer respectively to the center of mass longitudinal momentum and energy of the detected pion. It has also been shown[1] that the sparse data available for K and $\bar{p}$ production are consistent with this description. The observed scaling in terms of x_R is in contrast to the typical factors of 10 to 100 violation of scaling in the Feynman variable over the same energy range.

It is natural to inquire whether the cross sections scale in the limit $x_R \to 1$. This corresponds to the elastic reactions

$$\pi^{\pm} + p \to \pi^{\pm} + p$$

$$K^{\pm} + p \to K^{\pm} + p$$

$$\bar{p} + p \to \bar{p} + p$$

These reactions are completely unexplored at large momentum transfer ($|t| > 2$) and high energy. The experimental results on inclusive pion production demonstrate the importance of making the elastic measurements over the largest possible energy range at large fixed momentum transfer.

II. Physics Objectives and Justification

The purpose of this experiment is to measure the elastic scattering of $\pi^{\pm}$, $K^{\pm}$, $\bar{p}$ at 50, 100, 200, 300 and 400 GeV for $|t| \gtrsim 2$ $(GeV/c)^2$. The upper limit of momentum transfer will be determined by the counting rate and the lower limit (which could be less than 2 $(GeV/c)^2$) by the desire to provide a region of overlap with existing data. Experiment 7 (Meyer et al.) presently has data out to $|t| > 1$ $(GeV/c)^2$ and expect to approach $|t| = 2$ $(GeV/c)^2$.

The lower limit of the elastic cross section which will be able to be measured will be less than 10^{-36} $cm^2/(GeV/c)^2$ and the experiment will be able to place an upper limit to the cross section at large $|t|$ of $\sim 10^{-37}$ $cm^2/(GeV/c)^2$. The energy dependence of the elastic cross section, $d\sigma/dt$ at fixed $|t|$ follows a power law behavior[2] s^{-n} (where n depends on $|t|$). The value of n decreases as s is is increased (Fig. 1) until the cross section scales. However, at ISR energies the pp elastic cross section at $|t| \gtrsim 2$ $(GeV/c)^2$ dramatically changes its character and begins to rise although at this time the statistics are poor. The

increase in cross section appears to be about a factor of 2 over the ISR energy range.[3] These preliminary results are shown in Fig. 2. This behavior was predicted in 1972 within the context of the Impact Picture[4] and is connected with the rising proton proton total cross section. More generally, the s dependence of the elastic cross section provides model independent information on the impact parameter range which is responsible for the increasing total cross sections.

As the K^+p total cross section starts to rise already at 20 GeV this channel is of great interest in providing the cleanest means of studying the mechanisms involved in the phenomenon of rising cross sections. It is likely that the kaon-nucleon elastic cross secion at large momentum transfer is quite large and will therefore be relatively easy to measure. The simplest way to see this is by observing that the Kp total cross section is small, 20 mb, compared to 30 mb and 40 mb for πp and pp respectively. This implies that the kaon probably is quite a small object compared to the pion and nucleon and this will result in a larger scattering cross section at large momentum transfer. Figure 3 shows the prediction[5] of the Impact Picture for K^+p elastic scattering and the preliminary data of Exp. 7. Already at $|t| = 1$ there is a strong suggestion that the Kp cross section is becoming much larger than the pp cross section. Figure 4 shows the predicted pomeron contribution to each elastic cross section in the range $0 \leq |t| \leq 10\ (\mathrm{GeV}/c)^2$.

For $s > 600\ \mathrm{GeV}^2$ the pp predictions are in good agreement with the ISR data out to $|t| \simeq 4(\mathrm{GeV}/c)^2$. The predicted Kp cross section flattens out at large $|t|$ and is about $10^{-36}\ \mathrm{cm}^2/(\mathrm{GeV}/c)^2$ at $|t| \simeq 20\ (\mathrm{GeV}/c)^2$. Although these Kp estimates may be somewhat optimistic they do raise the definite possibility of making measurements out to enormous momentum transfer.

We therefore take note of the following:

1. The Kp channel may have more than a thousand times the cross section of the other channels at large $|t|$. Although the K content of the beam is expected to be rather small ($K/\pi \sim .1$) it is possible that the number of scattered kaons will be large relative to pions. This is in distinct contrast to the situation for single particle inclusive production at large $P_\perp$ where the kaons are less numerous than pions. For this reason we propose to have full π-K separation of the scattered particles in order to obtain an initial survey of the cross sections. Based on the results of the survey we will respond to any large particle ratios by adding additional particle identification if necessary.

2. The spectrometer system should be physically able to measure to a $|t|$ of at least $15(\mathrm{GeV}/c)^2$.
3. There will probably be significant s-dependencies of the "asymptotic" cross sections, $d\sigma/dt$, as in the pp channel. To study this will require measurements over the largest possible energy range.

We now summarize the physics objectives of this experiment. We shall measure the elastic cross sections for the processes

$$\pi^{\pm} + p \rightarrow \pi^{\pm} + p$$
$$K^{\pm} + p \rightarrow K^{\pm} + p$$
$$\bar{p} + p \rightarrow \bar{p} + p$$

from 50 to 400 GeV, $|t| \gtrsim 2(\mathrm{GeV}/c)^2$. The lower limit of cross section which will be measurable will be about $10^{-37}\ \mathrm{cm}^2/(\mathrm{GeV}/c)^2$. These reactions are of fundamental importance. They will provide information on the mechanism of rising total cross sections. In addition, many model predictions (parton etc.) exist which try to relate the strong interaction dynamics of inclusive particle production and elastic scattering in the high momentum transfer region. The data obtained from this experiment together with the available

inclusive data will provide stringent constraints for such models.

III. Experimental Method

A. General

Our objective is to be sensitive to the lowest possible cross sections. For this purpose we need to use the highest beam intensity available, a long target and have the largest possible detector acceptance. The importance of the latter requirement is greatest for 300 and 400 GeV running because of the decreasing particle flux in the beam. For this reason we have designed our spectrometers to have a very large acceptance. At the same time, however, we have taken care to ensure that detectors are located in such a way that their instantaneous singles counting rates are acceptable.

Figures 5 and 6 show the Laboratory angles of the recoil proton (approximately independent of incident beam particle species and momentum) versus $|t|$ and the angle of the fast forward scattered particle versus $|t|$. Given that a major part of the running for the experiment is required for the largest $|t|$ measurement we have chosen to design our magnet spectrometers with very large ϕ acceptance and at the same time have a large Δt acceptance at large $|t|$. In fact, the recoil proton is detected with high efficiency in the range $5.7 \leq |t| \leq 12.7$ $(\mathrm{GeV}/c)^2$ in a single setting with a $\Delta\phi$ acceptance of 30°. This

$|t|$acceptance transforms to $\Delta\theta_{Hor} = 0.37^{\circ}$ and $\Delta\phi_{Vert.} = 30^{\circ}$ for the forward scattered particle at 200 GeV/c incident energy. The small geometric acceptance for the forward scattered particle is of help not only in limiting the cost of the forward magnets but in keeping to a reasonable radius the very long Cerenkov counters required for momenta above 200 GeV. In addition, we can see from Fig. 6 that if we scale distances proportional to energy for the forward spectrometer then we maintain full acceptance over the energy range 50-400 GeV.

The measurements will be made using an intense ($\sim 10^9$ particles/sec) unseparated secondary beam of hadrons produced from a primary proton beam of up to 500 GeV/c. This beam intensity precludes counting in the incident beam. The liquid hydrogen target will be 16" long.

Elastic events will be defined by measuring the momentum and angle of both particles in the final state using magnetic spectrometers. This provides a one constraint fit for elastic scattering even though no measurements are made in the incident beam. The forward scattered particle will be identified with Cerenkov counters. Figure 7 shows a layout of the two spectrometers.

The momentum resolution in the forward arm will be $\lesssim \pm 1\%$ or better in all cases and $\lesssim \pm 1.5\%$ in the recoil spectrometer. The recoil arm will have an angular

resolution of ± 2.5 mr, and the forward arm an angular resolution of ± .25 mr at 100 GeV and proportionately better at the higher energies. These provide quite adequate t resolution ($\Delta t/t \lesssim .03$), and enable tight kinematic constraints to be made to reject backgrounds.

B. Recoil Spectrometer

Recoil protons will be analyzed using a magnet which bends trajectories in the vertical plane (see Figure 8). Proportional wire chambers will be located behind the magnet. A trajectory will be defined by the chambers behind the magnet together with the line source defined by the beam in the target. This magnet will have a 15 Kg field and will be 60" long, with a 24" pole width and a 15" gap. To enable this magnet to be as close as possible to the target at the small angles ($\sim 30^{\circ}$ for $|t| \simeq 10$ $(\mathrm{GeV/c})^2$), the incident beam passes through a slot in one of the pole pieces. The effect of the pole piece slot on the magnetic field is slight. The coils are carried around on the other side of the aperture.

Proportional chambers P_1, P_2 will have vertical wires with 3 mm spacing and will be separated by 3 feet. The angle of the recoil proton is measured to an accuracy of $\Delta\theta_p = \pm 2.4$ mr. Proportional chambers P_3 and P_4 have horizontal wires with 2 mm spacing and are used to determine the recoil momentum. The chambers are separated by 3' giving a magnet exit angle resolution of ± 1.6 mr.

The hodoscopes H_1 and H_3 have 1" fingers in the vertical direction and allow measurements of the recoil proton angle to ± 20 mr. Hodoscopes H_2 and H_4 have 2" fingers in the horizontal direction and provide a measurement of the recoil proton magnet exit angle to ± 30 mr. The hodoscope information is used in the trigger as described later.

This spectrometer, when set at ~ 32° to the beam line, for the large $|t|$ measurements, has an acceptance of $\geq \pm 2.5^{\circ}$ in the horizontal plane for the entire target length and a $\Delta\phi$ acceptance of 30°. The target acceptance of the spectrometer as a function of $|t|$ is shown in Fig. 9. Three settings will be required to cover the full range $2 \leq |t| \leq 12.7$ $(\mathrm{GeV/c})^2$ with a $\Delta\phi$ acceptance of $\geq 20^{\circ}$ and a target acceptance of $\gtrsim 60\%$ for all $|t|$. The acceptance over the entire $|t|$ range varies by $\lesssim 4\%$ within the $|t|$ resolution of the spectrometer.

The rms momentum and $|t|$ resolutions of the spectrometer are summarized in the table below. When we take into account the ± 1 mr beam divergence, the multiple scattering of the recoil proton in the target and the finite target size we obtain:

Recoil Spectrometer Resolution

$\lvert t \rvert$ $(GeV/c)^2$	$\frac{\Delta p}{p}$	$\frac{\Delta t}{t}$
2	± 0.6%	± 1.0%
6	± 1.2%	± 1.1%
10	± 1.8%	± 1.2%

C. Forward Spectrometer

The forward scattered particle will be analyzed in a vertical bending magnet with proportional wire chambers P_5, P_6, P_7 and P_8 in front and P_9 and P_{10} behind the magnet. To sweep (see Fig. 10) lower momentum charged particles away from the front chambers, a small vertical-bending magnet (~ 6" gap x 3" pole width x 72" long) will be placed close to the target. The line source defined by the beam in the target together with P_5, P_6, P_7 and P_8 will provide a second momentum measurement. Although the resolution on this measurement is somewhat poorer than in the main analyzing system, it will be helpful in eliminating any pole tip scatters which escape the other cuts in the trigger and analysis.

The main momentum-analyzing magnet will be 6.5" gap x 9.5" high x 20' long and will be constructed as shown in Fig. 10 to allow close enough approach to the beam. The distance of this magnet from the target will be scaled to the incident energy, so that the distances from the beam for fixed $|t|$ will remain the same. The

acceptance is matched to that of the recoil arm at large $|t|$.

The proportional wire chambers P_5, P_6, P_7, P_8, P_9, and P_{10} will have 1 mm wire spacing and permit an rms angle measurement of ± .2 mr at 100 GeV/c (resolution scales with energy) and an rms momentum determination of ± 1%. Hodoscopes H_5, and H_6 allow a measurement of the scattering angle to ~ ±1 mr and H_7 and H_8 measure the azimuth to $\leq 10^{\circ}$. Both of these resolutions include the beam divergence which dominates the estimates. The horizontal element hodoscopes H_9 and H_{10} are located behind the analyzing magnet. The information from the hodoscopes is used in the trigger as described later.

Threshold Cerenkov counters C_1 and C_2 are shown in the 200 GeV configuration in Fig. 7. Counter C_1 detects pions and C_2 detects both pions and kaons. Simultaneous identification of pion, kaon and nucleon scattering can thereby be achieved. It is quite possible that the predicted large differences in cross sections will make the task of particle identification very difficult. For example if the K/p cross section is indeed > 10^3 at large $|t|$ then a small inefficiency in counter C_2 will give a large error to the nucleon cross section.

If on the other hand, the large differences in cross section are not found, then the relatively small K/π ratio of the beam (~ .1) probably prevents measuring

the K cross section below $\sim 10^{-35}$ cm^2, that is, at the highest energies and largest $|t|$. In this case, we need only identify pions with reasonable efficiency ($\gtrsim$ 95%).

The Cerenkov counters shown in Fig. 7 will provide reliable cross section measurements for both pions and kaons in either of the above situations. C_1 is 65 meters long giving an efficiency for pion detection of $\varepsilon_\pi \simeq 99.9$; C_2 has a comparable efficiency for kaons and is 25 meters long. These efficiencies guarantee that for either extreme, in relative cross section, the contamination of K's in the π signal or π's in the K signal is $\lesssim$ 3%. This is certainly adequate and may be relaxed somewhat.

Depending on the results of the early running, we will add whatever additional particle identification that is necessary.

D. Trigger

We intend reaching a cross section sensitivity of $\frac{d\sigma}{dt} \sim 10^{-37}$ cm^2/(GeV/c)^2. In a $\Delta t = 1$ (GeV/c)^2, this corresponds to about one interaction in every 10^{11} beam target interactions being an elastic event. Hence a high rejection efficiency for background processes is required in the trigger. We propose using a three level trigger system. The first level employs a fast

coincidence between hodoscopes

$$H_1 \cdot H_2 \cdot H_3 \cdot H_4 \cdot H_5 \cdot H_6 \cdot H_7 \cdot H_8 \cdot H_9 \cdot H_{10}$$

and a calorimeteric measurement of the forward energy to 25%.

The second level of the trigger employs a hardwire matrix coincidence of the hodoscope information. Assuming elastic kinematics, coplanarity to within $\pm 5^{\circ}$ can be demanded. In addition, the hodoscope reconstruction can assure that the tracks in both arms are target associated. If these requirements are met, the hodoscope information will be used to mask the proportional chambers for track finding in the final level of trigger definition.

In the third and final trigger level, a hard-wired processor of the proportional chamber outputs will be employed to make

i) a coplanarity check to $\pm 3^{\circ}$,

ii) forward momentum determination to $\pm$ 10%,

iii) recoil angle-momentum correlation to $\pm$ 10%.

The first level trigger signal will be processed in about 100 ns. The coarse hodoscope logic will require an estimated 200 ns (roughly the gating time of the chambers). The last level of the trigger involves track

location within "roads" generated by the hodoscopes and will require an estimated 1 μs.

If all three levels of trigger are satisfied then a master trigger signal will be generated and all counter and wire chamber data will be recorded on magnetic tape.

A schematic description of the hodoscope data filter and proportional chamber processor is given in Appendix II, and their effect on the trigger rate is outlined in Section VI.

IV. Beam Requirements

The highest possible beam intensity is required within the constraints given below. Our detection system is designed to be able to accomodate 10^9 incident particles/ beam pulse.

The vertical beam spot size should be $\leq$ 2 mm so as not to degrade the momentum resolution of the recoil arm. The vertical beam divergence should be kept to ± 0.4 mr at 100 GeV and proportionately less at higher energy to maintain the resolution in coplanarity for $|t| < 5$ $(GeV/c)^2$. The divergence can be increased to ± .6 mr for the large $|t|$ measurements at full beam intensity. The horizontal divergence should be less than ± 0.5 mr for the measurements with reduced beam intensity at low $|t|$. However, for measurements at the largest $|t|$ values which require maximum beam flux we can take a horizontal beam divergence of ± 1 mr.

V. Elastic Rates

The rate of elastic events is

$$N_{el} = N_\pi \, N_p \, \frac{d\sigma}{dt} \, \Delta t \, \frac{\Delta\phi}{2\pi}$$

N_π = beam flux = 1.2×10^{14} (300 hours, 9 sec. rep. rate, 10^9 π/pulse

N_p = target protons = 16.8×10^{23} (16" LH_2)

$\Delta\phi$ = azimuthal acceptance = 30°

At the cross section limit of 10^{-37} $cm^2/(GeV/c)^2$ we obtain ~ 2 events/$(GeV/c)^2$.

If we take as an estimate of the cross sections the lower limits predicted by the Impact Picture as shown in Fig. 4 then we expect to measure the πp cross sections to a $|t|$ of at least 5 $(GeV/c)^2$ at the highest energy and to $|t|$ of at least 15 $(GeV/c)^2$ for the kaons at all incident momenta.

The following table shows the predicted rates based upon the impact picture estimate of the minimum cross section (i.e. pomeron contribution only) that will be observed. This assumes a beam intensity of 10^9 pions/pulse (4×10^{11} π/hour and K/π=.1.

MINIMUM EXPECTED RATES

t $(GeV/c)^2$	$\Delta\phi$	$d\sigma/dt$ $cm^2/(GeV/c)^2$ πp	kp	Time (Hours)	Yield/$(GeV/c)^2$ πp	kp
2.5	20°	$1x10^{-33}$	$8x10^{-31}$	100	4,000	320,000
5.0	25°	$2x10^{-36}$	$1x10^{-32}$	200	20	10,000
8.5	30°	$6x10^{-39}$	$5x10^{-34}$	300		800

Due to the expected small number of $\bar{p}$'s in the beam ($\bar{p}/\pi \sim 10^{-2}$) $\bar{p}p$ elastic cross section will be measured only to $\sim 10^{-34}$ $cm^2/(GeV/c)^2$.

VI. Backgrounds and Trigger Rate

The major background contaminations in the trigger of the proposed experiment are expected to result from quasi-elastic N* production and from random coincidences. The rates and system acceptance for these backgrounds is outlined below.

A. Quasi-Elastic N* Production

Events of the type $\pi p \rightarrow \pi N^*$ most nearly simulate elastic kinematics and will certainly provide acceptable triggers. Kinematically, this is most severe for the higher mass N*'s decaying in the production plane. The integrated diffractive inelastic cross section is known to be comparable to the elastic cross section. However, if we assume pessimistically that the N*'s, which appear to be produced in a

diffractive fashion at low energy, individually have production cross sections at $2 \lesssim |t| \lesssim 6$ $(GeV/c)^2$ comparable to the elastic cross section, then we will observe a somewhat greater number of N* events than elastics in the first level of the trigger. Less than 20% of the quasi-elastic events will satisfy the coplanarity and recoil angle-momentum correlation cuts in the third level of the trigger. The expected master trigger rate for this type of event is therefore comparable to or less than the elastic rate.

The angular and momentum resolutions of the recoil spectrometer are adequate to separate the decay proton from an elastic proton in the offline analysis for all but a small region of c.m. decay angles for the N* (for example, $\Delta\theta_{cm} \sim 20^{\circ}$ for the N* (1520)) and a small region in azimuthal angle of the decay plane ($\Delta\theta \sim 40^{\circ}$). Based upon these considerations, we expect to observe roughly 1% of the N* decays which are kinematically inseparable from elastic scatters within the system resolution. Assuming the integrated N* production cross section is comparable to the elastic cross section in this $|t|$ interval, we expect that the contamination will be about 1% in all cases and will simultaneously be measured in the kinematic region outside the elastic peak. This will allow a reliable subtraction to be made.

B. Singles Rates

Estimates of the single particle rates in the counters

have been made by scaling the invariant $pp \rightarrow \pi^o + x$ cross section by the πp to pp total cross section and integrating over the momentum and solid angle acceptances of the spectrometer arms. The $pp \rightarrow \pi^o + x$ cross sections used in the calculation are those measured in Experiment 63A and parametrized in the factorized form

$$E \frac{d\sigma}{d^3p} = A(1-x_R)^4 \exp(-BP_\perp + CP_\perp{}^2)$$

where

$A = 60 \text{ mb}/(\text{GeV}^2/c^3)$

$B = 5.0/(\text{GeV}/c)$

$C = 0.4/(\text{GeV}/c)^2$

$x_R = P^*/P^*_{max}$

The table below summarizes the instantaneous hodoscope rates resulting from this calculation assuming a beam intensity of 10^9 pions/machine cycle and a 1 sec spill. The rates were calculated for the large $|t|$ geometry at 200 GeV/c and includes equal contributions from both π^+ and π^- production.

Instantaneous Singles Rates per Second
for 1 Sec Spill

Recoil Spectrometer		Forward Spectrometer			
H_1, H_2	H_3, H_4	H_5, H_7	H_6, H_8	H_9	H_{10}
60K	24K	60K	55K	15K	2K

The singles rates in the detectors will be increased by nontarget associated events. Room background will be most severe for the large detectors in the recoil

spectrometer. These effects will be reduced to a tolerable level by shielding.

Secondary target backgrounds will be most severe in the forward arm where the solid angle subtended by the detectors from the target is small relative to the solid angle of the possible secondary targets. The most serious secondary targets will be the recoil spectrometer magnet structure, the beam pipe and the sweeping magnet poles. The sweeping magnet in the forward spectrometer will shield the detectors quite well from the recoil magnet structure. It may be desirable to use a helium bag instead of a beam pipe between the target and downstream detectors. Pole tip scatters in the forward spectrometer will certainly increase the singles rates in the detectors. This could provide an increase in singles rates by as much as a factor of 5 or 10 in H_5, H_6, H_7 and H_8. We do not expect a correspondingly large increase in the detectors H_9 and H_{10} behind the analyzing magnet due to the large sweeping power of this magnet and the dominance of low momentum secondaries resulting from the pole tip scatters. Thus, no counter is expected to operate at more than about 0.5 megacycle per second instantaneous rate.

C. Trigger Rate

The trigger rate (at any level of the trigger) will consist primarily of elastic scatters, quasi-elastic production and random coincidences. As discussed in part

A of this section, we expect the quasi-elastic rate satisfying the full trigger to be comparable to or less than the elastic rate. We shall now estimate the random coincidence rate for the trigger.

The rate of random coincidences between the hodoscopes in the recoil and forward spectrometers is determined by the rates of particles traversing the complete set of detectors in both spectrometers. As discussed in Section B above, these rates will be dominated by the single particle inclusive rates and are 24 K and 2 K respectively. Assuming a 10 ns resolving time we will therefore obtain ~0.5 random coincidences/machine cycle. The three level trigger system will reduce this to about 0.1 random master trigger/hour. This has been estimated in the following way.

Less than 30% of the random coincidences among the hodoscopes will satisfy the calorimetric energy measurement in the forward spectrometer. Thus ~0.13 randoms/pulse will satisfy the first level of the trigger.

In the second trigger level ~30% of the randoms will satisfy the coplanarity cut (~0.04/pulse). In addition, at this level most nontarget associated tracks will be eliminated.

In the third and final level of the trigger 40% of the randoms will survive the coplanarity cut and assuming a momentum distribution ~exp(-5.0 $P_\perp$) in both spectrometers, a further reduction by at least a factor of 50 is realized in the momentum cuts and the angle-momentum

correlation in the recoil spectrometer. We then expect ~0.1 random master trigger/hr which is quite satisfactory. The master trigger rate is therefore dominated by at least a factor of a thousand by elastic and quasi-elastic scattering at the large $|t|$ setting.

VII. Time Request

We propose to divide the experiment into two phases. In the first phase (Phase I) we will study

a) the $|t|$ dependence of the $\pi^{\pm}p$, $K^{\pm}p$ and $\bar{p}p$ elastic cross section for $2 \lesssim |t| \lesssim 12.7$ $(GeV/c)^2$ at 200 GeV. As indicated in the yield calculation, this will require 600 hours of beam.

In addition, we will investigate

b) the s dependence of these cross sections by obtaining data at 100 and 400 GeV in the interval $3.5 \lesssim |t| \lesssim 7.0$ $(GeV/c)^2$.

Less than 200 hours will be required at each of these two energies. The total time required to perform these measurements is then $\lesssim$ 1000 hours. We will also require 200 hours for testing and tuning.

Based upon the results of the Phase I experiment we will request time for Phase II. There we will perform a more detailed study of the s dependence of the cross sections by running at 50, 100, 300, and 400 GeV/c for momentum transfers up to the largest $|t|$ that the rates permit.

In summary, the Phase I running time request is

Secondary Beam Energy	Hours of Beam Time
100 GeV	200 hours
200 GeV	600 hours
400 GeV	200 hours

together with 200 hours of tune up time.

VIII. FermiLab Requirements

We propose that the items listed below be provided by the Laboratory research facilities.

1. Liquid hydrogen target 16" long.
2. Three magnets and the associated mechanical support systems. Approximate design characteristics and cost estimates for the magnets are given in Appendix I.
3. PREP electronics.
4. Computer and Porta Kamp.
5. Shielding and collimation as necessary.

The Physics Departments of FermiLab, Northeastern University, and Northern Illinois University will provide

1. Beam Monitors
2. Cerenkov counters
3. Scintillation counters

4. Proportional chambers

5. Hardwire data processors (Appendix II)

IX. Proposed Schedule

From the time of approval of this proposal we can have the apparatus assembled and ready for preliminary testing in 18 months. No technological development work is required for any of the apparatus; the design is straightforward and can be done now. We believe that the high momentum transfer elastic scattering results obtained through this experiment will be crucial to our understanding and progress in strong interactions. For these reasons, i.e. a) fundamental physics interest and b) technological straightforward design, we request prompt action and support of this proposal.

X. Additional Experimental Possibilities

The spectrometer system proposed here is well suited to experiments other than the large $|t|$ elastic scattering. Two of the more interesting possibilities are discussed briefly below.

A. Backward Elastic Scattering

With the addition of a short Cerenkov counter for particle identification in the recoil spectrometer, the large $|u|$ ($1 \lesssim |u| \leq 12$ $(\mathrm{GeV}/c)^2$) elastic scattering reactions

$$\pi^{\pm} + p \rightarrow p + \pi^{\pm}$$
$$K^{\pm} + p \rightarrow p + K^{\pm}$$
$$\bar{p} + p \rightarrow p + \bar{p}$$

can be studied. In fact because mass effects are essentially negligible at high energy and momentum transfer, our optimized high $|t|$ double spectrometers are also optimal for the high $|u|$ case. The same remarks can be made for the interesting crossed reactions

$$\bar{p} + p \rightarrow \pi^- + \pi^+$$

$$\bar{p} + p \rightarrow K^- + K^+$$

Little is known about the high energy behavior of any of these cross sections. At large s and u, baryon exchange amplitudes typically become small so parton effects may dominate.

Compared to the first generation backward scattering experiments proposed in the Meson Laboratory this study would be approximately 1000 times more sensitive in looking at small cross sections.

B. Inclusive Reactions

The inclusive particle production cross sections in the reactions

$$\pi^{\pm} + P \rightarrow \left.\begin{array}{l} \pi^{\pm} \\ K^{\pm} \\ p^{\pm} \\ \phi^{o}(K^{+}K^{-}) \\ \ldots \end{array}\right\} + X$$

and the corresponding reactions for $K^{\pm}$ and $\bar{p}$ projectiles can be studied at large transverse momentum.

Particle identification would be required in the incident beam and this would limit the flux to ~10^7 particles/sec. Beam intensity can be controlled by using particles produced at a $p_\perp$ ~1 GeV/c and thereby enhancing the kaon and anti-proton content of the beam. For 10^7 particles/pulse we would obtain about 3×10^6 K/pulse.

The forward spectrometer would be operated in its largest solid angle position corresponding to about 0.35 msr. This large solid angle allows the detection of the decay products of short lived particles such as the ϕ, K_S^o, etc. In addition, it is conceivable that useful correlations could be studied when triggering on specific particles in the forward spectrometer and using the large aperture second spectrometer to study the reaction products.

Inclusive cross sections would be measured out to $p_\perp$ ~ 5 GeV/c and over a large range of center of mass angle.

APPENDIX I

Magnet Parameters and Cost Estimate

The table on the following page shows the basic design parameters for the three magnets discussed in this proposal. Based upon these parameters rough designs have been generated in order to provide an estimate of the cost of each magnet. The cross sections of the magnets shown in Figures 8 and 10 are based on this design and some of the pertinent numbers are included in the following table. The cost estimates are based on a machined steel price of $400/ton and a formed copper price of $8/lb. These estimates do not include assembly cost.

Upon approval of this experiment we will attempt to locate existing magnets or parts of magnets which can be adapted for our use. In particular, the sweeping magnet geometry is not critical and a suitable substitute can probably be found. The 20' analyzing magnet has a larger aperture than the main ring bending magnets, but it may be possible to modify and use some of the parts without excessively compromising the experimental design.

Magnet	Recoil Spectrometer Analyzing Magnet	Forward Spectrometer Sweeping Magnet	Forward Spectrometer Analyzing Magnet
Central Field (Kg)	15	18	18
Gap (in.)	15	6	6.5
Field Width (in.)	24	3	9.5
Field Length (in.)	60	72	240
Coil turns	500	150	120
Current (Amps.)	1000	1500	2000
Conductor Cross Section (in.Xin.)	.6x.75	.5x.5	.5x.6
Power (KW at 30% Duty Factor)	46	60	100
Copper Weight (tons)	5.2	1.2	7.5
Steel Weight (tons)	33	3.2	21.4
Copper Cost (formed)	$83.2K	$19.3K	$120.0K
Steel Cost (machined)	$13.2K	$ 1.3K	$ 10.6K
Total Cost	$96.4K	$20.6K	$130.6K

APPENDIX II

ELECTRONIC DATA FILTER AND PROCESSOR DESCRIPTION

In order to improve the signal to noise ratio in the trigger of the proposed experiment we will design and build;

i) a hardwire data filter operating entirely on hodoscope information.

ii) a hardwire processor of multi-wire proportional chamber information.

This bi-level system will insure that the particles taking part in the fast trigger satisfy loose kinematic constraints before the event is recorded on tape. This will significantly reduce system deadtime and off-line processing time. The system will be designed to limit the trigger rate resulting from potentially serious types of backgrounds, namely random coincidences and nontarget associated tracks. An overall reduction in trigger rate by more than a factor of 100 will be realized for both of these types of events.

The detection system described earlier employs scintillation hodoscopes at all proportional chamber locations. This permits a) initial track candidate selection from the hodoscopes during the proportional chamber gating time and b) masking of the chambers with the hodoscopes, that is, examining the chambers for

"hits" in hodoscope selected regions of the chambers.

The first level of the trigger is defined by the presence of a coincidence between all hodoscope planes. On satisfying this loose trigger all hodoscope data will be latched into an equal-time fast hardware data register for further analysis. The analysis will proceed in two levels as described below until either

i) the trigger passes all tests and a computer interrupt is generated,

ii) a test failure occurs and the trigger is aborted or

iii) the trigger is determined to be ambiguous and a computer interrupt is generated by default.

A. Hodoscope Filter (Trigger Level II)

During the proportional chamber gating time the latched hodoscope data will be filtered to select master trigger candidates. The block diagram outlines the tests to which the hodoscope data is subjected. Each mask is a matrix of two sets of hodoscope elements hardwire programmed to fulfill certain coincidence requirements. The hodoscope pairs are examined to allow only acceptable trajectories through the magnets, collimators, etc. In addition, the hodoscope analysis includes a check on the azimuthal correlation of the

track candidates in the forward and recoil spectrometers. Filtered hodoscope data outputs of the masks contain only acceptable hits on each hodoscope plane. Each mask also generates a trigger (reset) signal if the coincidence requirements are (not) met.

The individual masks are technically straight forward to make and require ~ 3 logic levels. The overall decision time is therefore < 100 ns using emitter-coupled fast logic.

Immediately following the parallel masking, comparison of the filtered hodoscope data is performed to eliminate data which has not satisfied all masks in which the individual hodoscopes participate. This comparison requires at most 2 logic levels or roughly 50 ns. At this stage ambiguous events are defined as those in which more than one element of H_2, H_4, H_6, H_8, H_9 or H_{10} satisfies all masks. Ambigous events will result in a master trigger and computer interrupt.

For unambigous events satisfying all masks the filtered hodoscope data and a Level II trigger will be communicated to the proportional chamber processor.

B. Multi-Wire Proportional Chamber Processor (Level III)

The definition of single track candidates in the hodoscope filter simplifies proportional chamber processing and results in a significant saving in processing time. The chamber information is processed

primarily in order to improve the resolution on the trigger candidates and to check for recoil production angle and recoil momentum correlation. The block diagram outlines the essential features of the processor.

A trigger from the hodoscope filter initiates addressing and subsequent readout of the hodoscope defined regions of interest in MWPC planes P_2, P_4, P_6, P_8, P_9 and P_{10}. The chamber data is decoded to the forward and recoil spectrometer bend angles (momenta) and azimuths. These are parallel masked to insure

i) that the momenta are in the range of interest and

ii) that the tracks are azimuthally correlated.

In parallel with these masks, the recoil bend angle (momentum) is matrixed with the recoil production angle candidates. This preprogrammed hardwire matrix will pass only those H_1 H_3 combinations corresponding to a production angle which is consistent with the determined recoil momentum assuming elastic scattering kinematics. If more than one H_1 H_3 pair satisfies the mask, a default master trigger will result. A single H_1 H_3 pair will initiate readout of the corresponding P_1 P_3 regions. The production angle will be decoded and again masked with the recoil momentum.

The output of the processor will be a) a system reset if any mask fails or b) a master trigger and computer interrupt if all masks are satisfied or c) a default master trigger if more than one H_1 H_3 pair is found to agree with the calculated momentum (assuming the azimuth and forward bend angle masks are satisfied) or if any addressed chamber region contains more than one wire "hit". The complete processing of an event will require several μs.

The hodoscope filter and processing system described here will, as detailed in Section VI, result in a master trigger rate of ~ .1/hr for randoms and non-target associated events. This is an improvement by a factor of ~ 500 from the hodoscope coincidence rate in level 1 of the trigger. In the worst case if the hodoscope singles rates would increase by a factor of 20 over the calculated inclusive rate, the master trigger rate for these sources would increase to ~ 20/hour. Most of these would result from the default conditions in the hodoscope filter. Even in this case the elastic and quasi-elastic master triggers will dominate by a factor of 10 at the largest $|t|$ configuration.

Block Diagram - Multi-Wire Proportional Chamber Processor

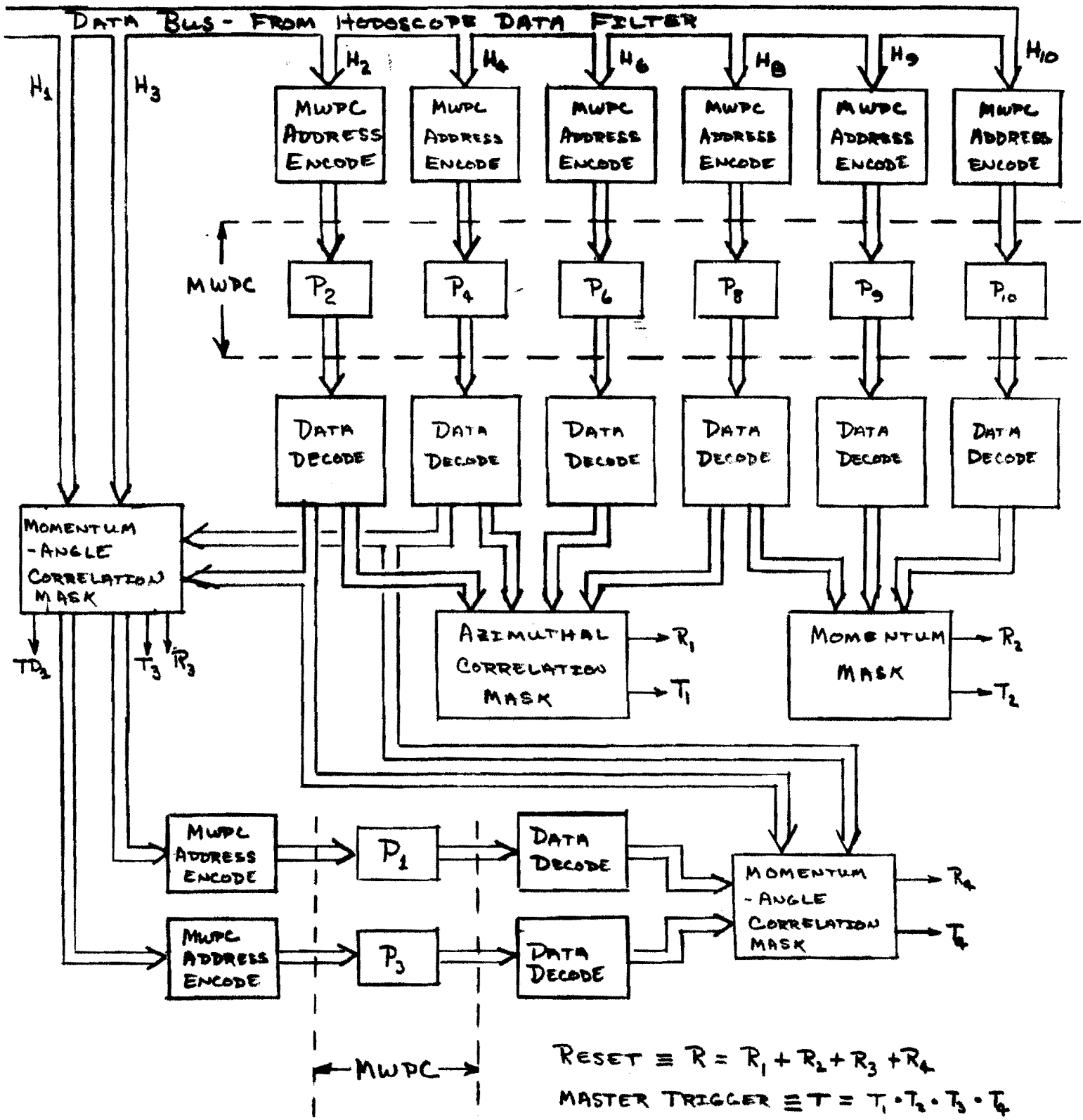

Reset $\equiv R = R_1 + R_2 + R_3 + R_4$

Master Trigger $\equiv T = T_1 \cdot T_2 \cdot T_3 \cdot T_4$

Default Master Trigger $\equiv TD = T_1 \cdot T_2 \cdot TD_2$

BLOCK DIAGRAM – HODOSCOPE DATA FILTER

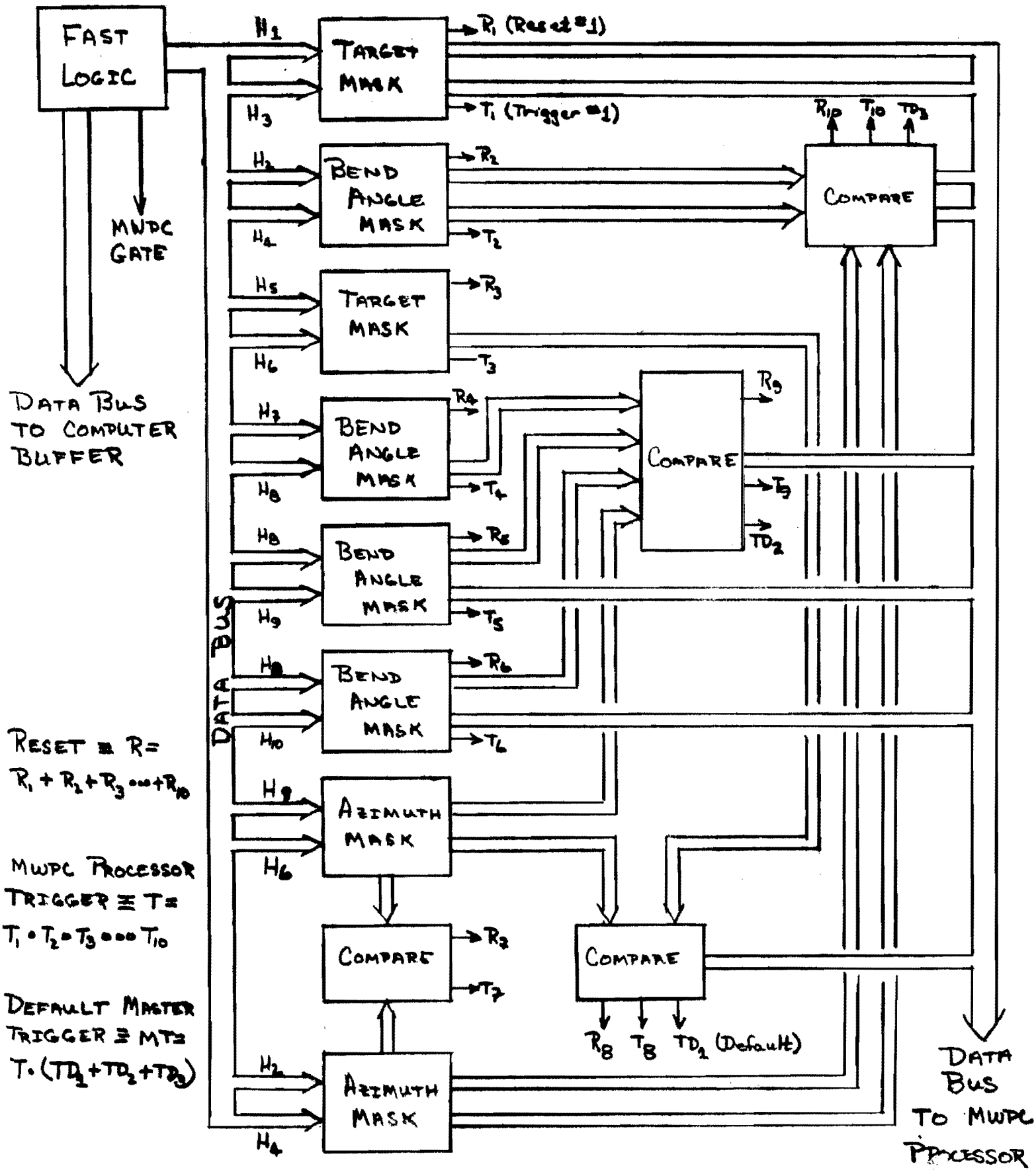

FIGURE CAPTIONS

Figure 1. Energy dependence of the pp elastic differential cross section at several fixed values of $|t|$.

Figure 2. Energy dependence of the pp elastic differential cross section in the region of the secondary maximum ($|t| \approx 2$ (GeV/c)^2) in the ISR energy region. A significant increase in the cross section at $\sqrt{s} \gtrsim 30$ is observed. The solid curve shows the s-dependence predicted by the Impact Picture.

Figure 3. Small $|t|$ K^+p elastic differential cross section as measured by Meyer et al. in (Fermilab Experiment 7). The curves are the predictions of the Impact Picture (Ref. 5). Some ISR pp elastic data is also shown.

Figure 4. Impact Picture predictions for the pomeron contribution to the πp and kp elastic cross section at 200 GeV/c. These are then the predicted minimum cross sections that will be encountered at 200 GeV/c.

Figure 5. Recoil proton laboratory angle vs. $|t|$ for πp elastic scattering. This curve is virtually energy independent (E > 50 GeV) and has little dependence on the type of forward scattered particle (k, $\bar{p}$).

Figure 6. Laboratory angle of the forward scattered

pion in πp elastic scattering at several fixed values of incident momentum.

Figure 7. Apparatus arrangement for the proposed experiment in the 200 GeV/c configuration.

Figure 8. Recoil spectrometer layout. The plan view in the upper left shows the 2 magnet poles, the 16" target and the beam line passing through the slot in the pole. Also shown are the approximate locations of the recoil arm detectors (hodoscopes and MWPC). The elevation view in the lower left shows the ray trace of 6 GeV/c particles at azimuths of $\pm 15^{\circ}$. The cross section of the magnet in the upper right shows the slot allowing close approach to the beam.

Figure 9. Calculated $|t|$ acceptance of the recoil spectrometer at the 3 settings required to cover the region $2 \leq |t| \leq 12.7$ $(\mathrm{GeV/c})^2$. The $|t|$ resolution of the spectrometer is such that the geometric acceptance does not change by more than ~ 4% within the resolution.

Figure 10. Layout of the forward spectrometer showing the target to the left, the sweeping magnet, momentum analyzing magnet, Cerenkov counters and the approximate detector locations. Below the two magnets are shown expanded cross

sectional views. The beam passes through the aperture of the sweeping magnet and a slot in the pole of the (vertical bend) analyzing magnet is provided for the beam pipe.

REFERENCES

[1]D. C. Carey, J. R. Johnson, R. Kammerud, M. Peters, D. J. Ritchie, A. Roberts, J. R. Sauer, R. Shafer, D. Theriot, J. K. Walker, and F. E. Taylor, Phys. Rev. Letters 33, 327, Phys. Rev. Letters 33, 330.

[2]D. Horn and F. Zacharism, Hadron Physics at Very High Energies, W. A. Benjamin Inc., Reading, Mass. (1973) and references cited therein.

[3]Results presented at the London Conference, July, 1974 by the Aachen-CERN-Geneva-Heidelberg-Turrin collaboration.

[4]H. Cheng, J. K. Walker, T. T. Wu, Paper presented to the XVI International Conference on High Energy Physics, Batavia (1972).

[5]T. T. Wu, Invited talk at the Fifth International Conference on High Energy Collisions, Stony Brook, N. Y., August, 1973.

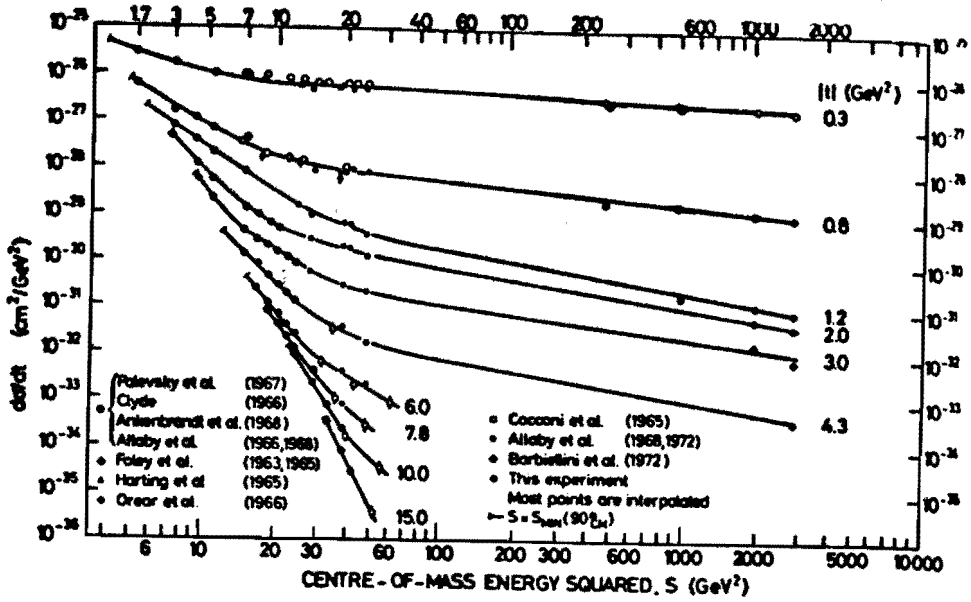

Figure 1

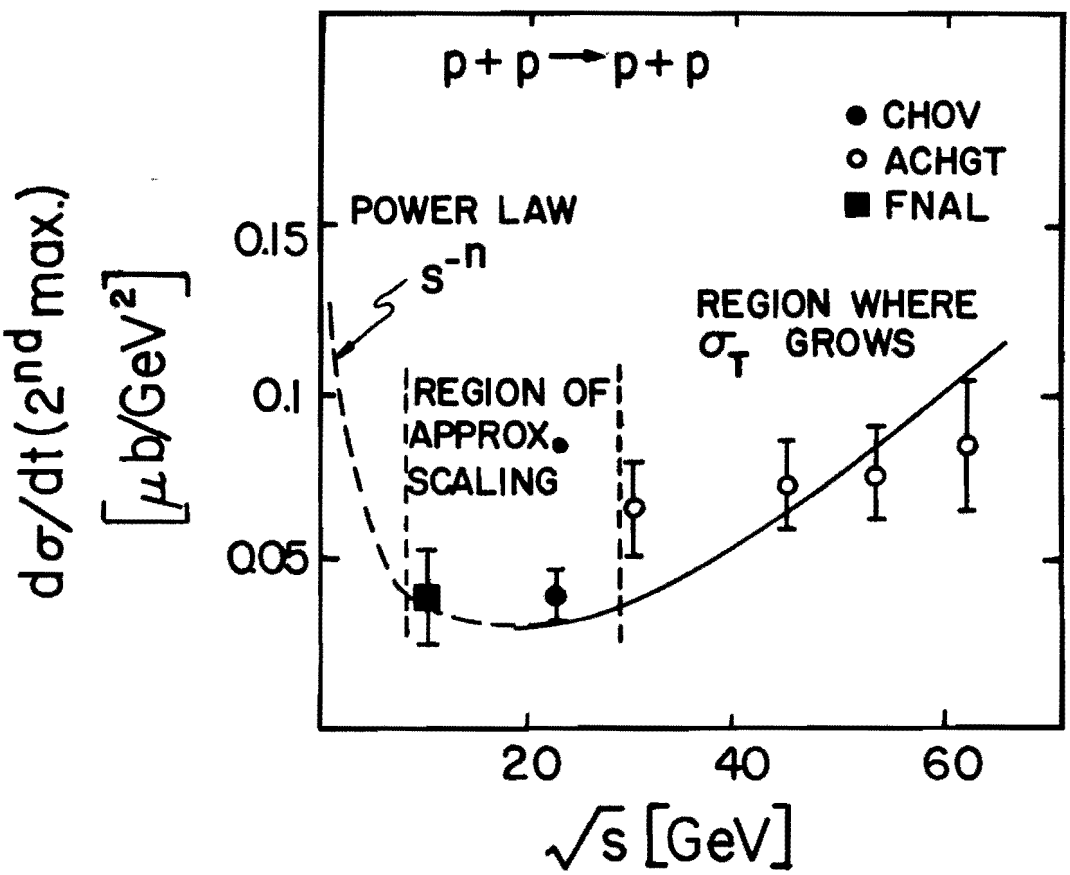

Figure 2

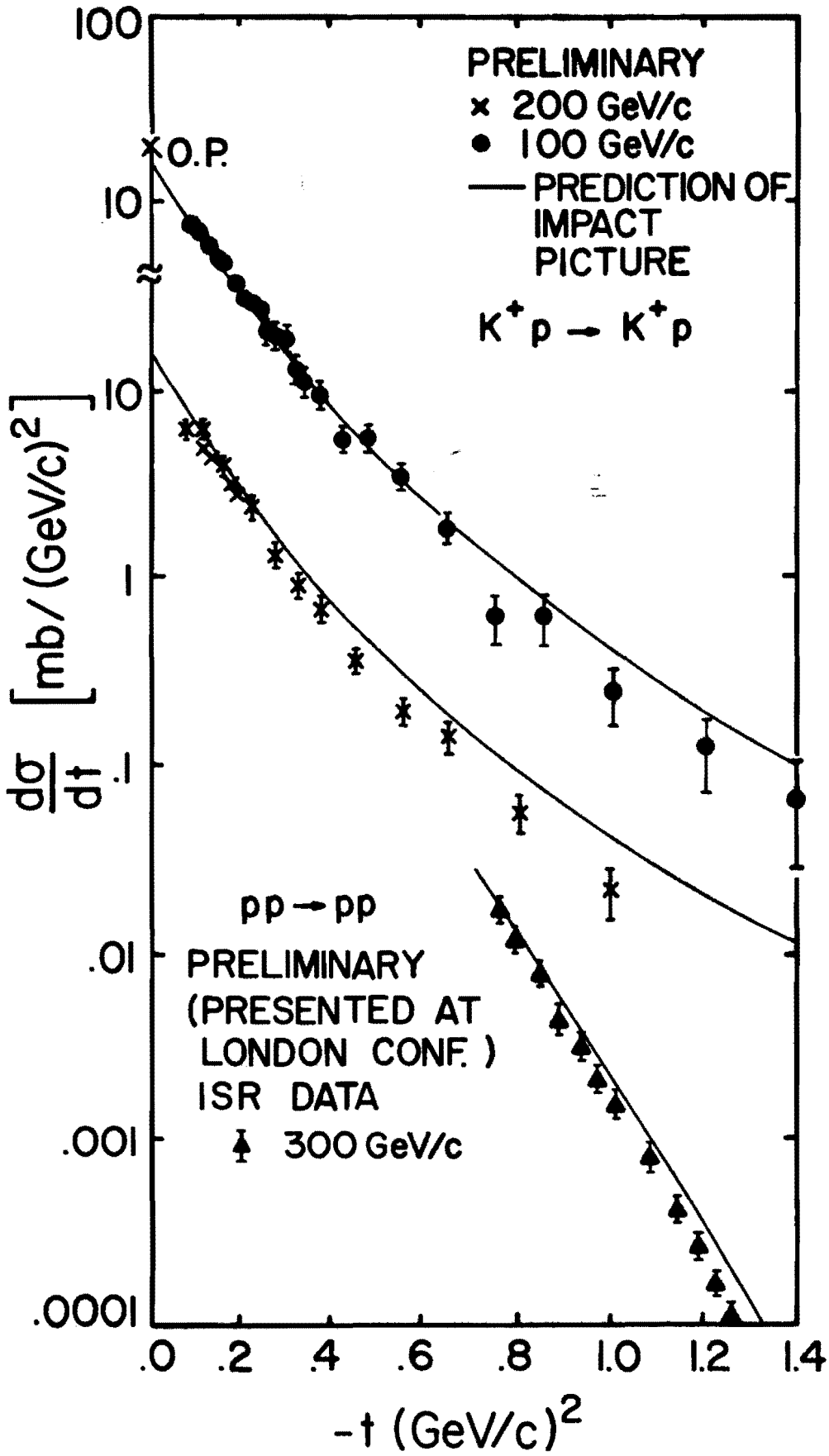
PRELIMINARY
× 200 GeV/c
● 100 GeV/c
PREDICTION OF IMPACT PICTURE
K⁺p → K⁺p
O.P.
pp → pp
PRELIMINARY
(PRESENTED AT LONDON CONF.)
ISR DATA
300 GeV/c
dσ/dt [mb/(GeV/c)²]
-t (GeV/c)²
100
10
10
1
.1
.01
.001
.0001
.0
.2
.4
.6
.8
1.0
1.2
1.4

Figure 3

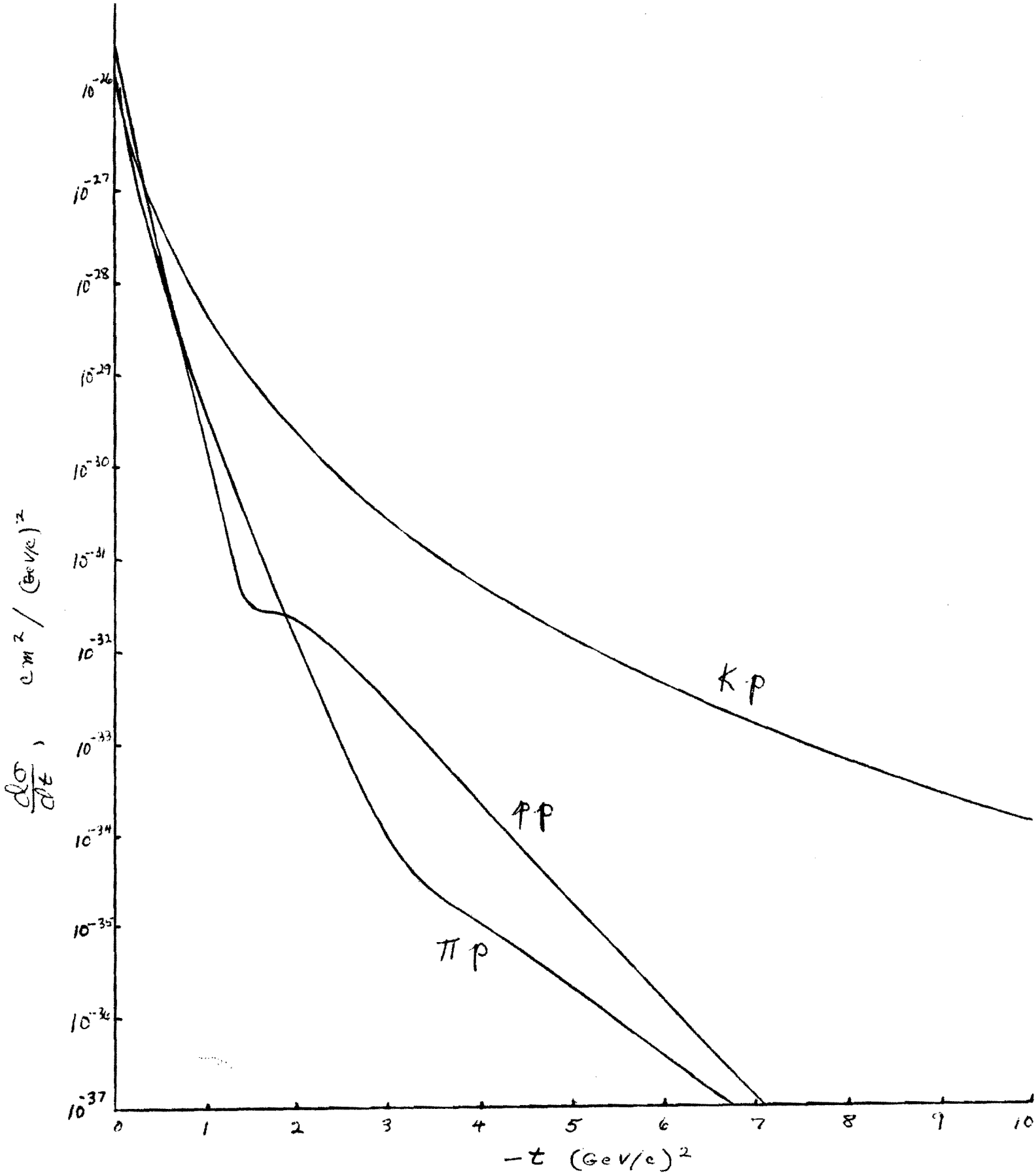
10^{-26}
10^{-27}
10^{-28}
10^{-29}
10^{-30}
10^{-31}
10^{-32}
10^{-33}
10^{-34}
10^{-35}
10^{-36}
10^{-37}
$\frac{d\sigma}{dt}$, $cm^2 / (GeV/c)^2$
0
1
2
3
4
5
6
7
8
9
10
$-t$ $(GeV/c)^2$
Kp
pp
πp

Figure 4

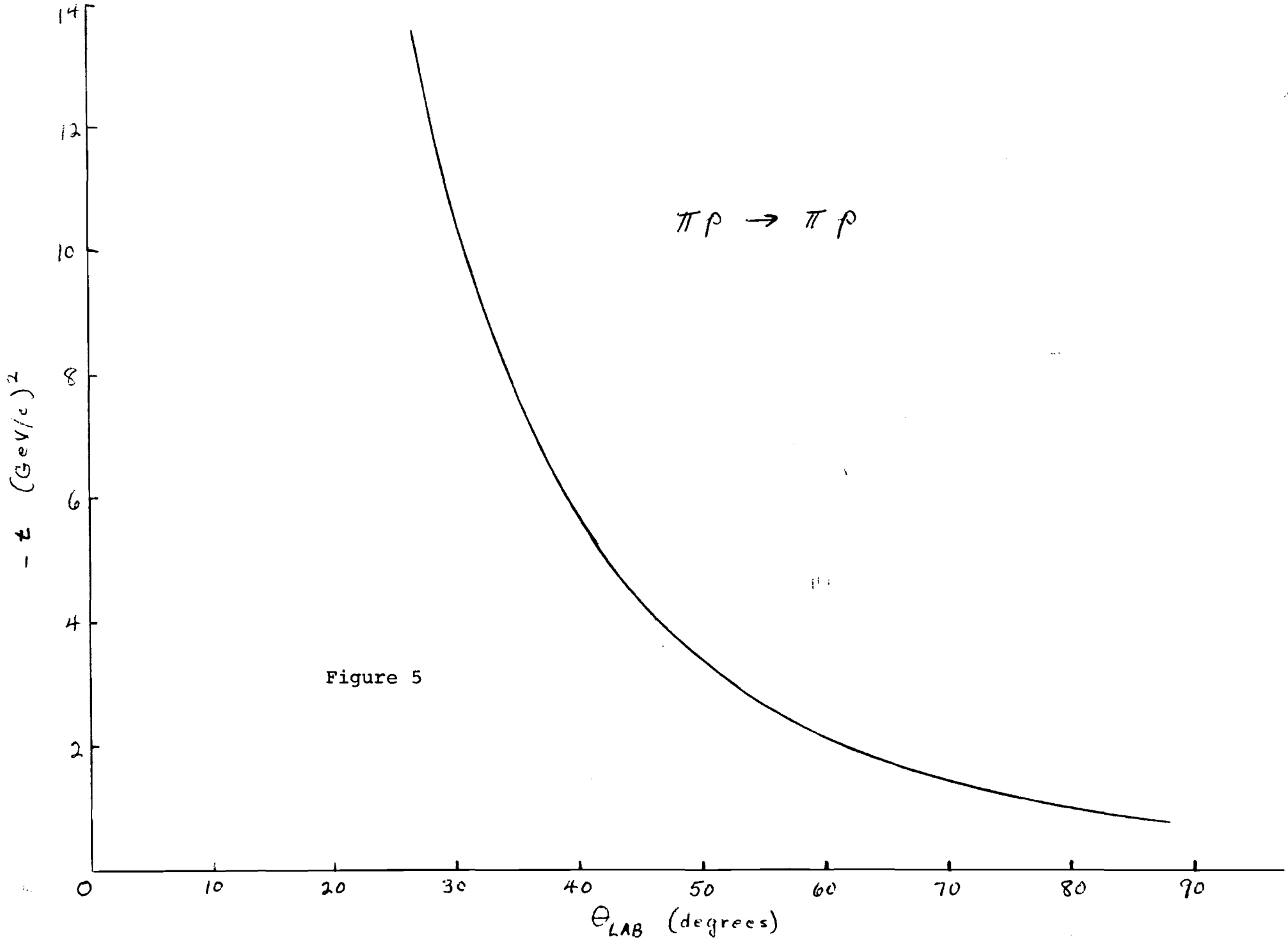
$\pi p \rightarrow \pi p$
$-t$ (GeV/c)^2
14
12
10
8
6
4
2
0
10
20
30
40
50
60
70
80
90
θ_{LAB} (degrees)

Figure 5

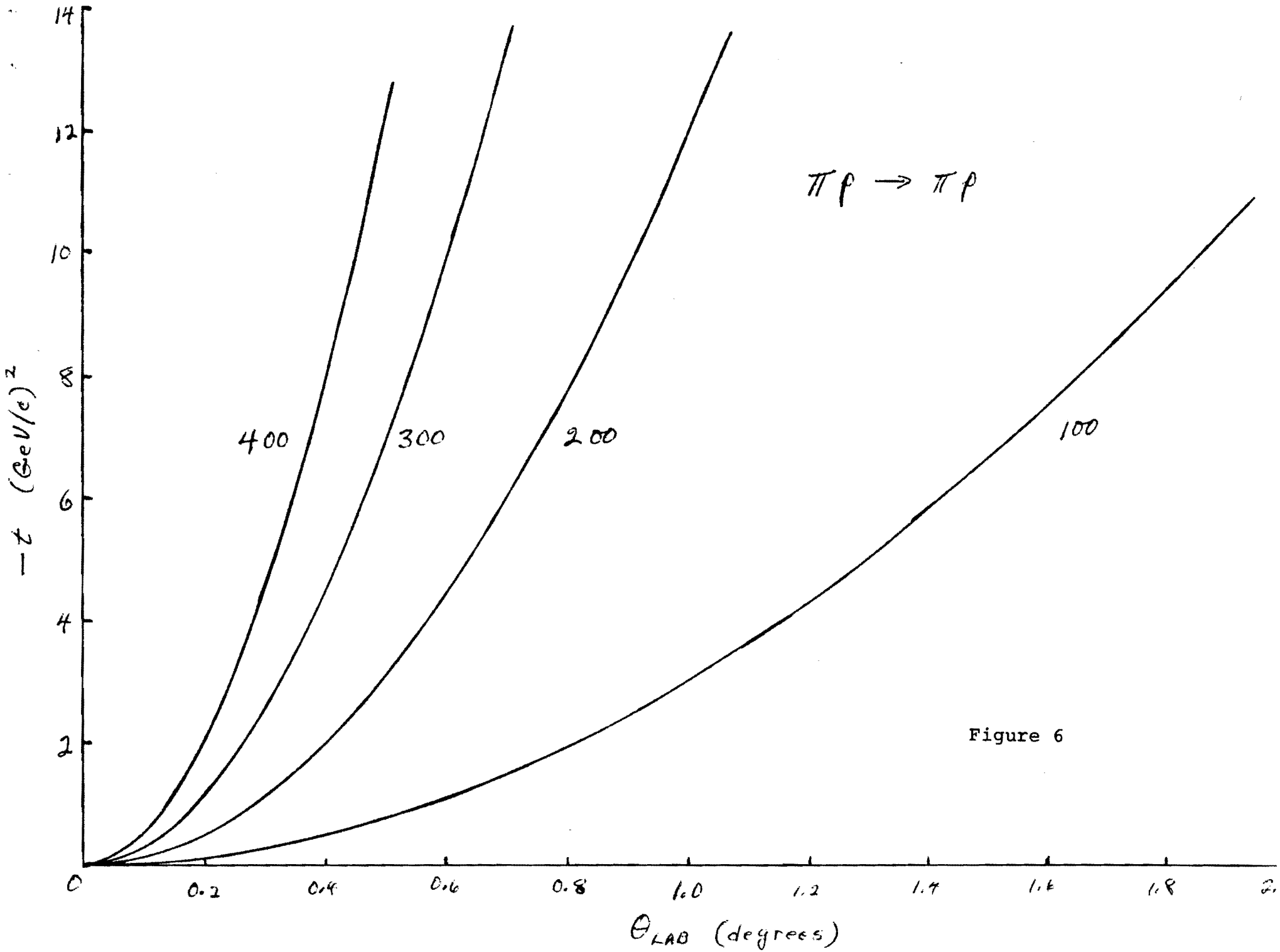
$\pi p \rightarrow \pi p$
400
300
200
100
$-t$ (GeV/c)^2
θ_{LAB} (degrees)
0
0.2
0.4
0.6
0.8
1.0
1.2
1.4
1.6
1.8
2.
2
4
6
8
10
12
14

Figure 6

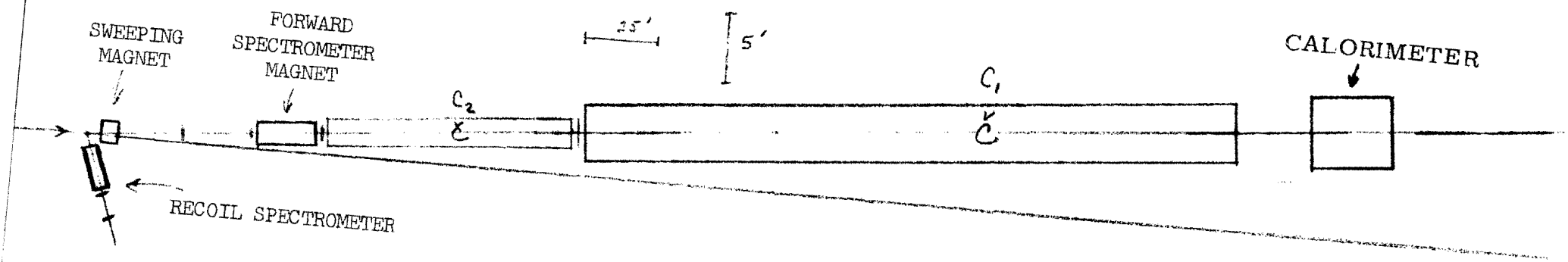
SWEEPING MAGNET
FORWARD SPECTROMETER MAGNET
25'
5'
C_2
C_1
CALORIMETER
RECOIL SPECTROMETER

Figure 7

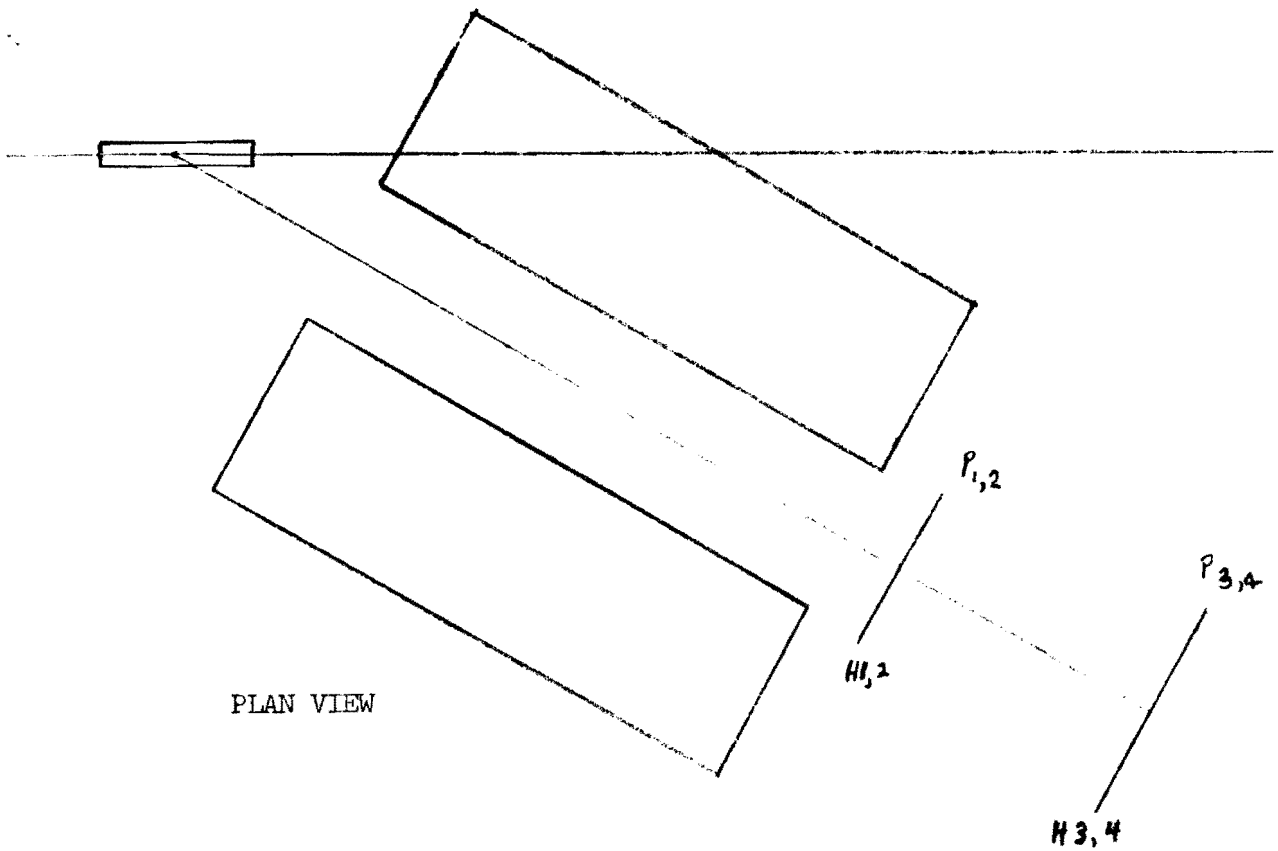

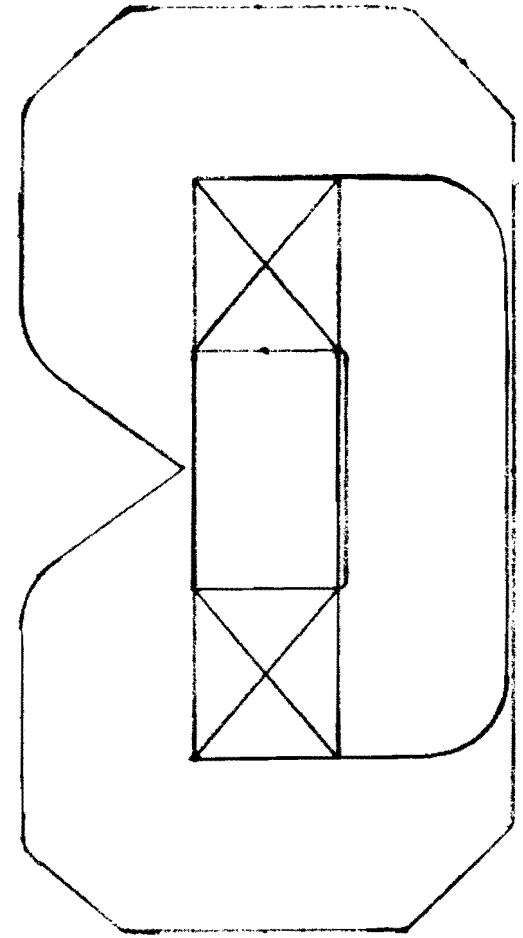

Figure 8

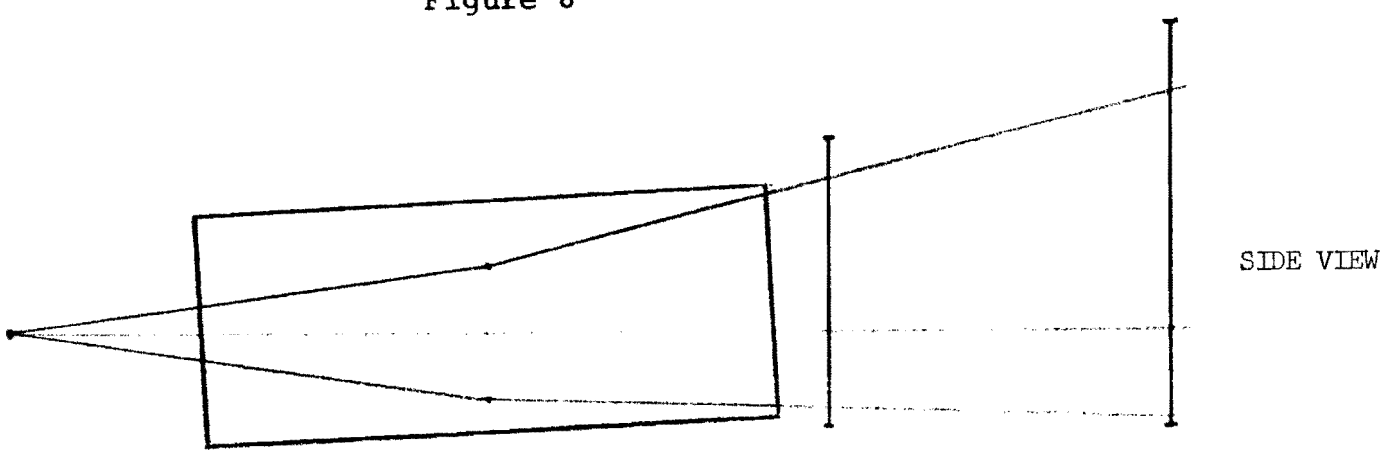

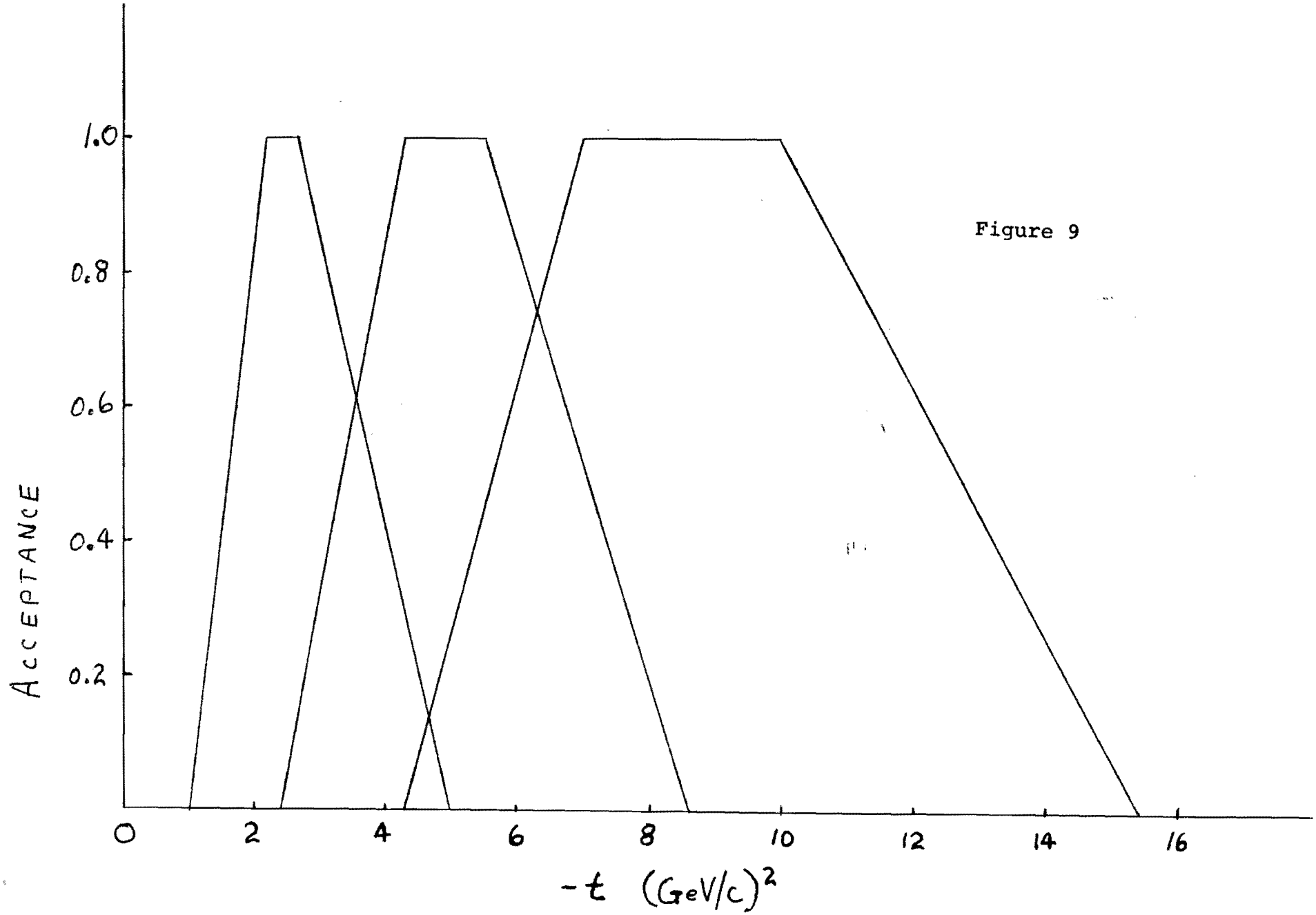

Figure 9

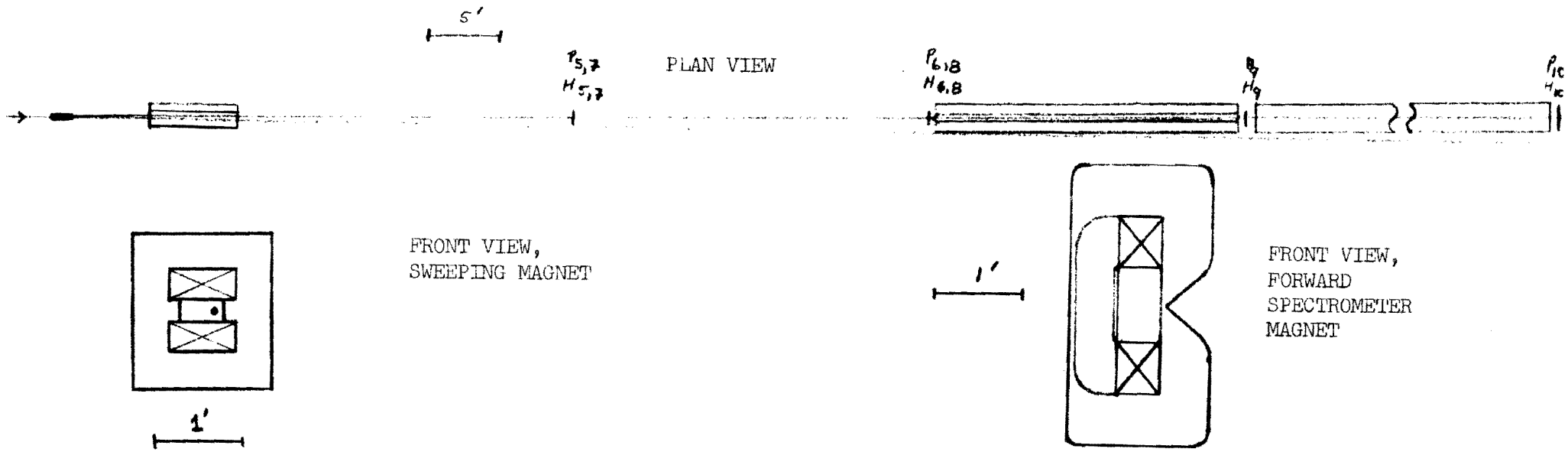
5'
$P_{5,7}$
$H_{5,7}$
PLAN VIEW
$P_{6,8}$
$H_{6,8}$
P_9
H_9
P_{10}
H_{10}
FRONT VIEW,
SWEEPING MAGNET
1'
1'
FRONT VIEW,
FORWARD
SPECTROMETER
MAGNET

Figure 10